Available online at www.sciencedirect.com

SciVerse ScienceDirect

Ceramics International 39 (2013) 6035–6040

CERAMICS INTERNATIONAL

www.elsevier.com/locate/ceramint

Fabrication of $CaSiO_3$ bioceramics with open and unidirectional macro-channels using an ice/fiber-templated method

Zhi Huang[a,b], Kechao Zhou[a], Dan Lei[a], Zhiyou Li[a], Yan Zhang[a], Dou Zhang[a,*]

[a]State Key Laboratory of Powder Metallurgy, Central South University, Changsha 410083, China
[b]Institute of Biomedical Engineering, School of Geosciences and Info-Physics Engineering, Central South University, Changsha 410083, China

Received 6 December 2012; received in revised form 26 December 2012; accepted 8 January 2013
Available online 17 January 2013

Abstract

Porous $CaSiO_3$ bioceramics with open and unidirectional macro-channels of pore size more than 200 μm are of particular interest for biomedical applications. An ice/fiber-templated method was employed for the fabrication of $CaSiO_3$ bioceramics with interconnected lamellar pores and macro-channels of pore size more than 200 μm. The pores formed by ice crystals transformed from cellular to lamellar, while the pores formed by fibers were aligned macro-channels, which were also in alignment with the lamellar pores. Keeping the initial slurry concentration constant and increasing the packing density of fibers, the volume fraction of macro-channels and open porosity increased, and the compressive strength decreased. Maintaining the packing density of fibers and increasing the initial slurry concentration, the pore sizes of lamellar pores and open porosity decreased, and the compressive strength increased. The results indicated that it was possible to manufacture porous $CaSiO_3$ bioceramics with the macro-channels of 250–350 μm, lamellae spacing of 50–100 μm, open porosity of 71.12–83.94% and compressive strength of 0.87–3.59 MPa, indicating the suitability for tissue engineering.

Keywords: B. Porosity; D. Glass; D. Silicate; E. Biomedical application

1. Introduction

Since the discovery of bioglass by Hench et al. in 1969, several glasses, ceramics and glass-ceramics have been regarded as bioactive ceramic materials [1,2]. $CaSiO_3$ (CS) has been synthetically prepared to be employed as bioactive ceramic material. Due to its excellent biocompatibility, osteoconductivity, controllable degradability and bioactivity, CS bioceramics have received significant attention for application in bone regeneration [3–5]. Recently, porous CS bioceramics have attracted increasing interest since they are characterized by a better bone-regenerative capacity and faster resorption rate in vivo compared to β-tricalcium phosphate [6]. To date, considerable attention has been paid to the development of fabrication methods for CS bioceramics in bone tissue engineering, including the polymer-sponge method [7–9], dry-powder processing with the addition of porogen [10], sol–gel and gel-casting [11]. However, how to prepare porous CS bioceramics with a controllable pore structure for bone tissue engineering still remains a challenge.

The ideal fabrication technique should produce complex-shaped bioceramics with controlled pore shape, orientation and size in a reliable and economical way [12]. Ice-templated method is a reliable and economical technique to produce porous complex-shaped ceramics [12,13]. In this process, an aqueous suspension is poured into a mold, frozen and then followed by sublimation of the ice. After sintering, a complex and often anisotropic porous microstructure with unidirectional channels is generated, and the final microstructure is a replica of ice [14]. The microstructure can be controlled by exploiting the physics of ice formation. However, owing to the physical limitation of ice formation, the ice-templated method is usually suitable to fabricate strong ceramics with small pores [15].

Scaffold architecture plays an important role in determining the degree and rate of bone ingrowth. Three commonly studied parameters are interconnectivity, porosity and the size of pore [16,17]. Interconnectivity and porosity in a

*Corresponding author. Tel./fax: +86 731 8887 7196
E-mail address: dzhang@csu.edu.cn (D. Zhang).

0272-8842/$ - see front matter © 2013 Elsevier Ltd and Techna Group S.r.l. All rights reserved.
http://dx.doi.org/10.1016/j.ceramint.2013.01.019

scaffold are absolutely required for nutrient and waste transport, and there is general agreement among researchers that an optimal pore size exists for successful host cell infiltration and tissue ingrowth: 5–15 μm for fibroblasts, 20–125 μm for adult mammalian skin tissue and 200–350 μm for bone tissue [18–21]. More recently, research has revealed that bioceramics with controlled-geometry, i.e., aligned macro-channels, had enhanced the degree and rate of bone ingrowth [22–24]. The incorporation of aligned macro-channels enhanced the permeability of bioceramics with an 18-fold increase and contributed to significant improvement of the initial distribution of cells. Furthermore, this structure can theoretically enhance core oxygen concentrations and prevent scaffold core necrosis, which are urgently needed for scaffold-based therapies [24]. Thus, it is necessary to develop effective methods to obtain macro-channels with pore size more than 200 μm in the scaffold.

For this purpose, porous CS bioceramics with macro-channels were fabricated using ice/fiber-templated method by fine-tuning the process parameters and the size and packing density of fibers, which were employed as the formation agents of macro-channels. The microstructures and mechanical properties of this novel porous CS scaffold were characterized and discussed.

2. Experimental procedure

Aqueous CS slurries with the initial concentration of 15 vol% and 20 vol% were prepared by mixing commercially available CS powders, deionized water and the dispersant ammonium polyacrylate (HydroDisper A160, Shenzhen Highrun Chemical Industry Co. Ltd., China). The dispersant concentration was 2 wt% with respect to the dried CS powders. The CS slurries were ball-milled for 48 h with zirconia media and de-aired in a vacuum desiccator. As shown in Fig. 1, the CS slurries were firstly poured into a polytetrafluoroethylene mold (10 mm diameter × 25 mm), in which polyethylene terephthalate fibers were arranged in parallel alignment. The diameters of the fibers were in the 300–450 μm range. The molds were then placed on copper cold fingers and kept at −30 °C with a freezing direction from bottom to top, in alignment with the direction of fibers. Upon solidifying, the fibers were pulled out from the frozen bodies. Finally, the frozen bodies were freeze-dried and sintered at 1100 °C for 3 h in air with a ramp of 5 °C/min.

The phase compositions were characterized using X-ray diffraction (XRD, Rigaku D/max-2550) with Cu Kα radiation (λ=0.15406 nm). A diffraction range of 10°–60° (2θ) was selected and the XRD analysis was carried out at 4°/min. To investigate the scaffold architecture and microstructure, the scaffold was embedded in epoxy for sectioning and polishing. SEM examinations were carried out with the use of environmental scanning electron microscopy (ESEM, Quantan 200, JEOL, Japan). The open porosity was measured using the Archimedes method. The compressive tests were carried out parallel to the freezing direction and measured using a mechanical testing machine (KD11-2, Shenzhen KEJALI Technology Co., Ltd., China) at a crosshead speed of 0.5 mm min^{-1}. To obtain the average porosity and compressive strength, five samples from each group were measured.

3. Results and discussion

3.1. Phase analysis

The phase structures of the as obtained CS powders and the CS ceramic sintered at 1100 °C for 3 h are shown in

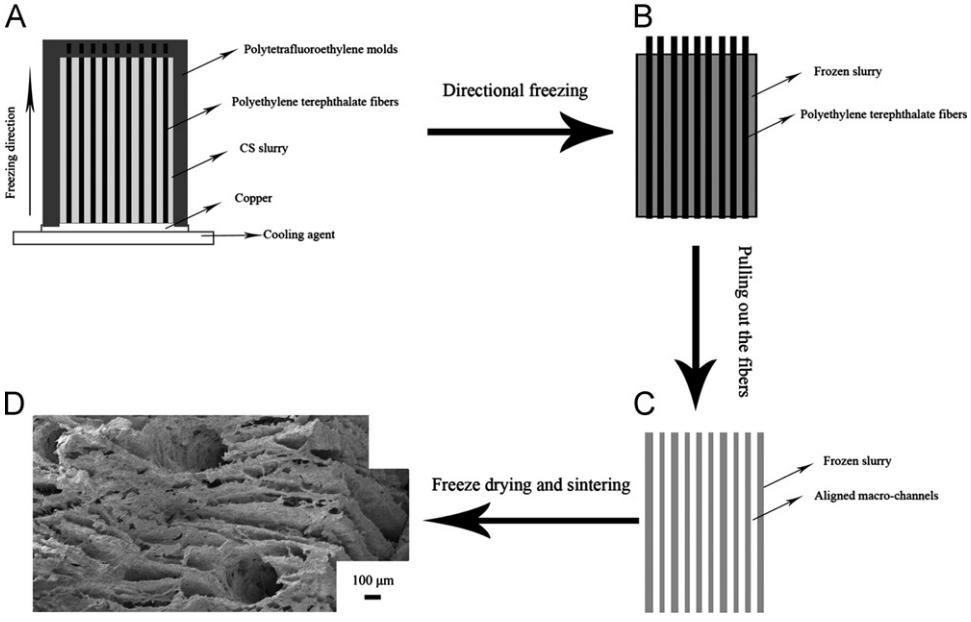

Fig. 1. Schematic of the ice/fiber-templated method. A: the setting up. B: the frozen body with embedded fibers. C: the frozen body after removing the fibers. D: the sintered CS bioceramics.

Fig. 2. It is clear to see from the diffraction patterns that the as-obtained powders were amorphous, whereas the ceramic sintered at 1100 °C for 3 h mainly consisted of β-phase CS.

3.2. General feature of the CS scaffold

As revealed by Fig. 3, the general microstructure of the CS scaffold was gradational and could be divided into Zone 1 and Zone 2. There existed macro-channels running through the scaffold, mixing with cellular pores in Zone 1 and lamellar pores at the edge of Zone 1 and in Zone 2. The macro-channel was formed by fibers, the cellular pores were formed by the initial randomly oriented ice crystals, and the lamellar pores were formed by lamellar ice crystals, which were oriented along the freezing direction. The transition of pore morphology from cellular to lamellar was not obvious. Unless explicitly stated, this paper focuses on Zone 2.

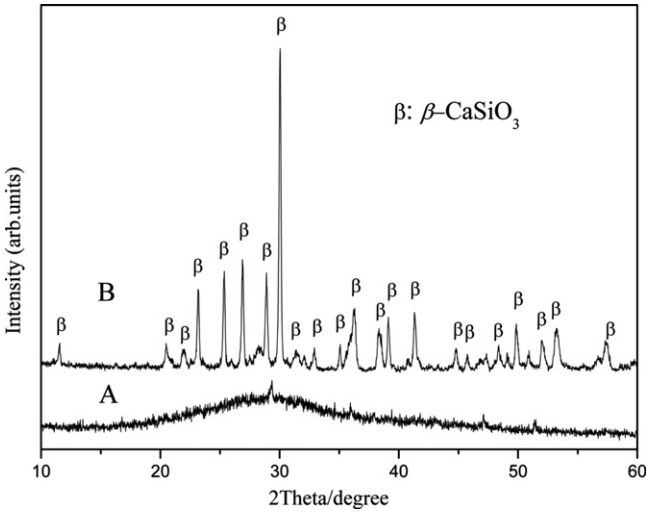

Fig. 2. XRD patterns of as obtained powders (A) and ceramics sintered at 1100 °C for 3 h (B).

The final porous architecture was the replica of fibers and ice crystals. Fundamentals of the physics of ice can help us to understand the underlying reason for this cellular to lamellar transition architecture. According to the crystal structure of ice and its crystal growth kinetics, hexagonal prisms were their most basic form. The growth of the facets parallel to the *a*-axis was kinetically favorable, and the ice growth rate along the *a*-axis was theoretically 100 times faster than that along the *c*-axis (perpendicular to the *a*-axis) [25–27]. Once the CS slurry was poured over a cold plate, nucleation of ice occurred rapidly and homogeneously near the cold surface due to a supercooling effect [28]. Ice crystals grew randomly and rapidly, and the CS particles were repelled and packed between the randomly oriented ice crystals, leading to a cellular pore structure. In these experiments, a temperature gradient existed in the slurry due to the directional freezing. After the initial rapid growth of ice crystals, the crystallization transformed into a steady state and ice crystals began to grow along the temperature gradient. As mentioned above, the growth of the facets parallel to the *a*-axis was kinetically favorable, so facets parallel to the *a*-axis kept growing along the temperature gradient, and the CS particles were compacted along the interface of ice crystals, leading to a lamellar microstructure. The fibers did not change during the whole freezing process, but were pulled out after freezing, leaving aligned macro-channels running through the scaffold. The macro-channels were also in alignment with the lamellar pores.

3.3. Control of the volume fraction of macro-channels

As shown in Fig. 4, the volume fraction of macro-channels could be controlled by varying the packing density of polymer fibers in the molds. The spaces that had been occupied by polymer fibers were turned into aligned macro-channels. With increasing packing density of polymer fibers in the molds, the volume fraction of

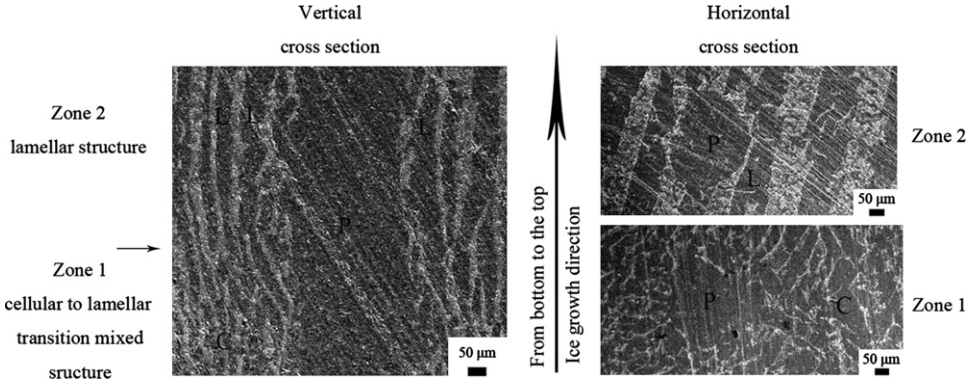

Fig. 3. SEM micrograph of the general microstructure of the bottom part (close to the copper cold finger) and evolution of the pore structure. The black portion in the micrograph is epoxy and the white portion is CS. Zone 1 is the transition region from cellular to lamellar, which can be clearly observed at the bottom of the scaffold (vertical cross-section, depicted on the left). Zone 2 is the lamellar region, which can be observed above Zone 1 (vertical cross-section, depicted on the left). The horizontal cross-sections of Zone 1 and Zone 2 are depicted at the lower right and the upper right; P: macro-channels formed by fibers; C: cellular pores formed by ice; and L: lamellar pores formed by ice.

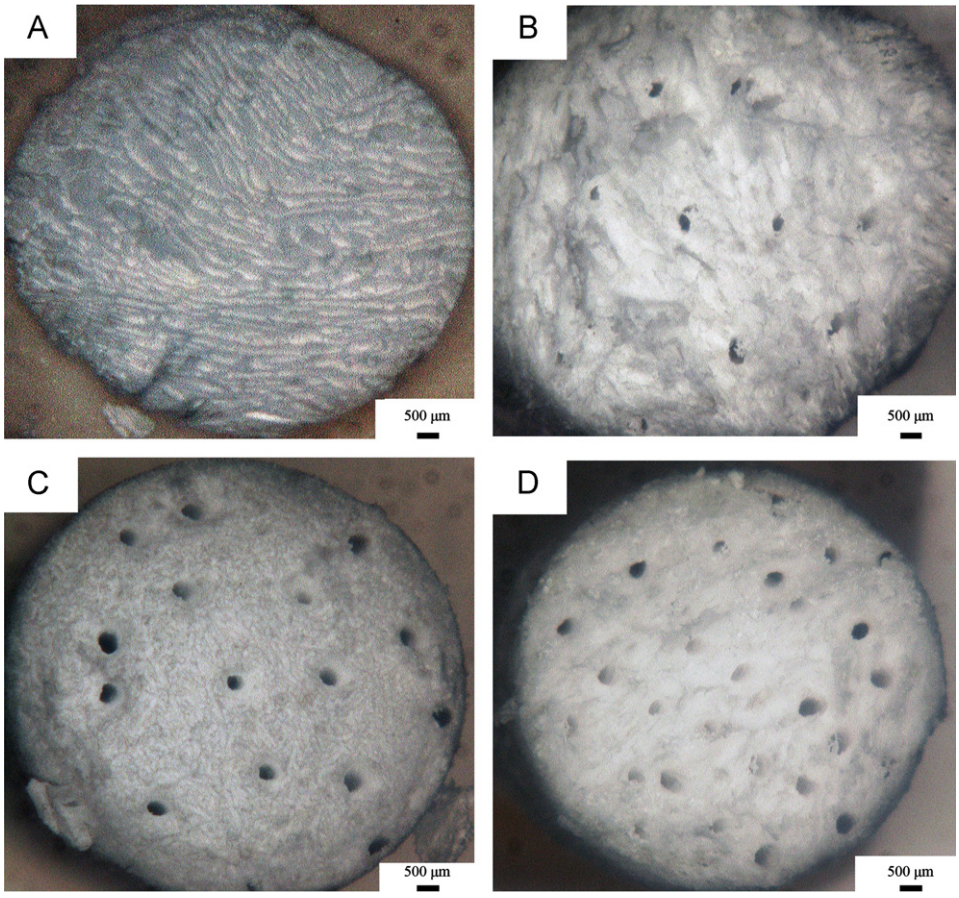

Fig. 4. Optical micrographs of the CS bioceramics fabricated by varying the packing density of fibers. A: no fibers; B: low density; C: middle density; and D: high density.

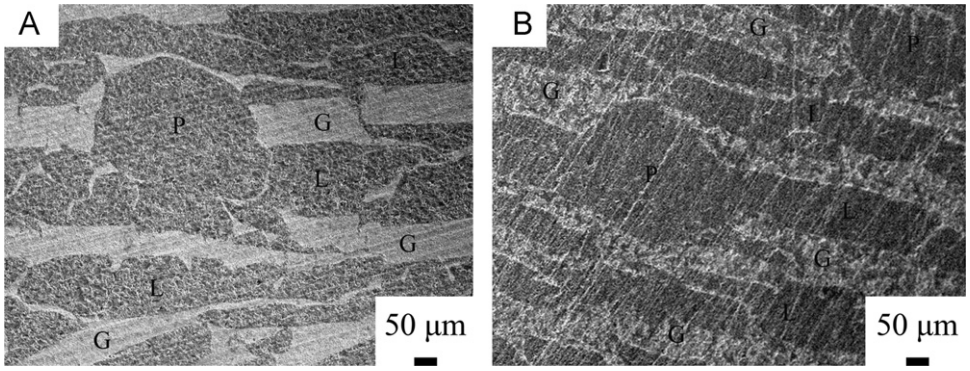

Fig. 5. SEM micrographs of the horizontal cross-section of the CS bioceramics fabricated by varying the initial slurry concentration. The black portion in the micrograph is epoxy and the white lamellar portion is CS. (A) 15 vol%; (B) 20 vol%. P: macro-channels formed by fibers; L: lamellar pores formed by ice; and G: CS ceramic wall.

macro-channels increased. The diameters of macro-channels were in the 250–350 μm range.

3.4. Control of the lamellar pores

As shown in Fig. 5, the lamellar pores were interconnected, and the pore size could be characterized by two-dimensional parameters: the long axis and the short axis. The short axis corresponded to the lamellae spacing. Larger lamellar spacing could be obtained at lower initial slurry concentrations. Samples with 15% initial slurry concentration had an average lamellae spacing of 100–200 μm, while those with 20% initial slurry concentration had an average lamellae spacing of 50–100 μm.

3.5. Control of the porosity and the compressive strength

Figs. 6 and 7 present porosities and compressive strengths of the CS bioceramics, respectively. The final porosities and compressive strengths could be tuned by changing the initial slurry concentration and the packing density of polymer fibers in the molds. An increase of the initial slurry concentration from 15 to 20 vol% caused the decrease of the final porosity, while the compressive strength increased. This was due to the fact that higher initial slurry concentration possessed lower water content and higher viscosity, thus produced lower lamellae spacing, porosity and higher compressive strength of the CS bioceramics. Under the same slurry concentration, an increase of the packing density of polymer fibers in the molds caused the increase of the final porosity, while the compressive strength decreased.

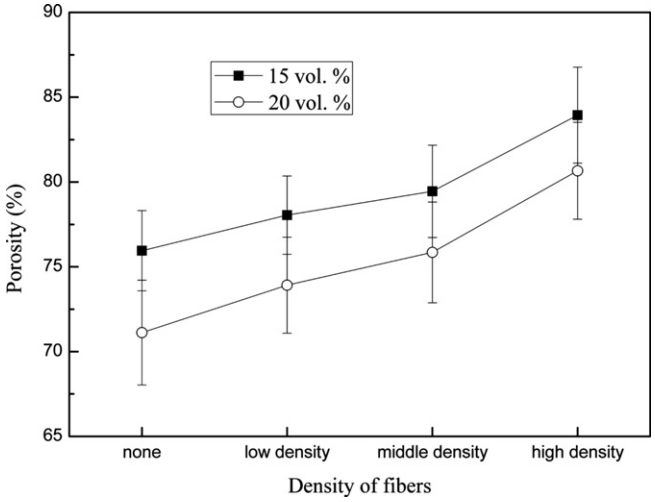

Fig. 6. Porosities of the CS bioceramics processed with 15 vol% and 20 vol% of initial slurry concentration vs. the packing density of polymer fibers in the mold.

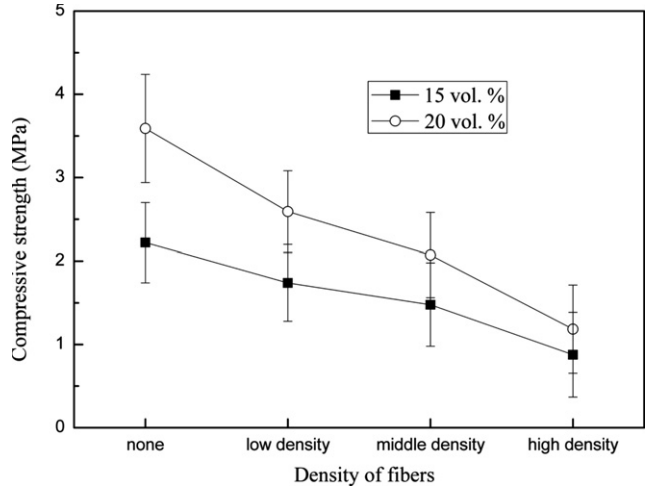

Fig. 7. Compressive strengths of the CS bioceramics processed with 15 vol% and 20 vol% initial slurry concentration vs. the packing density of polymer fibers in the mold.

The relationship between the porosity and strength behavior of porous ceramics could be approximated expressed by an exponential function [29]: $\sigma = \sigma_0 \exp(-cp)$. In the function, σ is the strength at pore volume fraction p, σ_0 is zero-porosity strength, and the constant c is related to the pore characteristics, such as pore size and shape. Thus, when the porosity (p) increased, the strength (σ) decreased sharply. Lin et al. [10] showed the compressive strength of the sintered porous CS with 53.35% porosity to be 7.64 MPa. Furthermore, Huan et al. [30] presented 0.28 MPa of the compressive strength of porous CS with around 83.1% porosity. In the present work, as the final porosity of the sintered porous CS bioceramics increased from 71.12% to 83.94%, the corresponding compressive strengths decreased from 3.59 to 0.87 MPa. Although the c parameters of these porous CS bioceramics were different, the strengths decreased as the pore volume fraction p increased.

4. Conclusions

In summary, the ice/fiber-templated method has been applied to fabricate porous β-CS bioceramics with interconnected lamellar pores and large macro-channels. The pores formed by ice crystals transformed from cellular to lamellar, while the pores formed by fibers were aligned macro-channels, which were also in alignment with the lamellar pores. Both the initial slurry concentration and packing density of fibers in the mold affected the microstructures and properties of the porous CS bioceramics. The diameters of macro-channels were in the 250–350 μm range. This ice/fiber-templated method covered the shortage of the ice-templated method and generated porous CS bioceramics, with interconnected lamellar pores and macro-channels of pore size more than 200 μm, indicating the suitability for tissue engineering.

Acknowledgments

This work was supported by the National Natural Science Foundation of China (No. 51172288), Hunan Provincial Natural Science Foundation of China (No. 11JJ1008), the Freedom Explore Program of Central South University (No. 2012QNZT075), China Postdoctoral Science Foundation (No. 2012M521564), and the Postdoctoral Science Foundation of Central South University.

References

[1] D. Bellucci, V. Cannillo, A. Sola, F. Chiellini, M. Gazzarri, C. Migone, Macroporous bioglass (R)-derived scaffolds for bone tissue regeneration, Ceramics International 37 (5) (2011) 1575–1585.
[2] H. Zhong, L. Wang, Y. Fan, L. He, K. Lin, W. Jiang, J. Chang, L. Chen, Mechanical properties and bioactivity of beta-Ca_2SiO_4 ceramics synthesized by spark plasma sintering, Ceramics International 37 (7) (2011) 2459–2465.
[3] L.L. Hench, The story of bioglass (R), Journal of Materials Science: Materials in Medicine 17 (11) (2006) 967–978.

[4] S.Y. Ni, J. Chang, In vitro degradation, bioactivity, and cytocompatibility of calcium silicate, dimagnesium silicate, and tricalcium. phosphate bioceramics, Journal of Biomaterials Applications 24 (2) (2009) 139–158.
[5] F. Barrera-Mendez, J.C. Escobedo-Bocardo, D.A. Cortes-Hernandez, J.M. Almanza-Robles, E.M. Muzquiz-Ramos, Gentamicin sulphate release from lost foam wollastonite scaffolds using poly(DL-lactide-co-glycolide) acid, Ceramics International 37 (7) (2011) 2445–2451.
[6] S. Xu, K. Lin, Z. Wang, J. Chang, L. Wang, J. Lu, C. Ning, Reconstruction of calvarial defect of rabbits using porous calcium silicate bioactive ceramics, Biomaterials 29 (17) (2008) 2588–2596.
[7] S.Y. Ni, J. Chang, L. Chou, A novel bioactive porous $CaSiO_3$ scaffold for bone tissue engineering, Journal of Biomedical Materials Research Part A 76A (1) (2006) 196–205.
[8] D. Bellucci, V. Cannillo, A. Sola, Shell scaffolds: a new approach towards high strength bioceramic scaffolds for bone regeneration, Materials Letters 64 (2) (2010) 203–206.
[9] C.V. Brovarone, E. Verne, P. Appendino, Macroporous bioactive glass-ceramic scaffolds for tissue engineering, Journal of Materials Science: Materials in Medicine 17 (11) (2006) 1069–1078.
[10] K.L. Lin, J. Chang, Y. Zeng, W.J. Qian, Preparation of macroporous calcium silicate ceramics, Materials Letters 58 (15) (2004) 2109–2113.
[11] J.R. Jones, L.L. Hench, Factors affecting the structure and properties of bioactive foam scaffolds for tissue engineering, Journal of Biomedical Materials Research Part B 68B (1) (2004) 36–44.
[12] S. Deville, E. Saiz, A.P. Tomsia, Freeze casting of hydroxyapatite scaffolds for bone tissue engineering, Biomaterials 27 (32) (2006) 5480–5489.
[13] K. Zhao, Y.F. Tang, Y.S. Qin, J.Q. Wei, Porous hydroxyapatite ceramics by ice templating: freezing characteristics and mechanical properties, Ceramics International 37 (2) (2011) 635–639.
[14] S. Deville, E. Saiz, R.K. Nalla, A.P. Tomsia, Freezing as a path to build complex composites, Science 311 (5760) (2006) 515–518.
[15] Y.M. Soon, K.H. Shin, Y.H. Koh, J.H. Lee, H.E. Kim, Compressive strength and processing of camphene-based freeze cast calcium phosphate scaffolds with aligned pores, Materials Letters 63 (17) (2009) 1548–1550.
[16] J.R. Woodard, A.J. Hilldore, S.K. Lan, C.J. Park, A.W. Morgan, J.A.C. Eurell, S.G. Clark, M.B. Wheeler, R.D. Jamison, A.J.W. Johnson, The mechanical properties and osteoconductivity of hydroxyapatite bone scaffolds with multi-scale porosity, Biomaterials 28 (1) (2007) 45–54.
[17] V. Karageorgiou, D. Kaplan, Porosity of 3D biomaterial scaffolds and osteogenesis, Biomaterials 26 (27) (2005) 5474–5491.
[18] A. Bignon, J. Chouteau, J. Chevalier, G. Fantozzi, J.P. Carret, P. Chavassieux, G. Boivin, M. Melin, D. Hartmann, Effect of micro- and macroporosity of bone substitutes on their mechanical properties and cellular response, Journal of Materials Science: Materials in Medicine 14 (12) (2003) 1089–1097.
[19] A.I. Itala, H.O. Ylanen, C. Ekholm, K.H. Karlsson, H.T. Aro, Pore diameter of more than 100 μm is not requisite for bone ingrowth in rabbits, Journal of Biomedical Materials Research 58 (6) (2001) 679–683.
[20] V.S. Komlev, S.M. Barinov, Porous hydroxyapatite ceramics of bimodal pore size distribution, Journal of Materials Science: Materials in Medicine 13 (3) (2002) 295–299.
[21] A. Macchetta, I.G. Turner, C.R. Bowen, Fabrication of HA/TCP scaffolds with a graded and porous structure using a camphene-based freeze-casting method, Acta Biomaterialia 5 (4) (2009) 1319–1327.
[22] M.M.C.G. Silva, L.A. Cyster, J.J.A. Barry, X.B. Yang, R.O.C. Oreffo, D.M. Grant, C.A. Scotchford, S.M. Howdle, K.M. Shakesheff, F.R.A.J. Rose, The effect of anisotropic architecture on cell and tissue infiltration into tissue engineering scaffolds, Biomaterials 27 (35) (2006) 5909–5917.
[23] H.S. Ryu, S.J. Kim, J.H. Kim, H. Kim, K.S. Hong, B.S. Chang, D.H. Lee, J.H. Lee, C.K. Lee, S.S. Chung, Fabrication of 1-dimensional porous hydroxyapatite and evaluation of its osteoconductivity, Journal of Materials Science: Materials in Medicine 15 (3) (2004) 267–273.
[24] C.T. Buckley, K.U. O'Kelly, Fabrication and characterization of a porous multidomain hydroxyapatite scaffold for bone tissue engineering investigations, J.ournal of Biomedical Materials Research Part B 93B (2) (2010) 459–467.
[25] S. Deville, Freeze-casting of porous ceramics: a review of current achievements and issues, Advanced Engineering Materials 10 (3) (2008) 155–169.
[26] W.L. Li, K. Lu, J.Y. Walz, Freeze casting of porous materials: review of critical factors in microstructure evolution, International Materials Reviews 57 (1) (2012) 37–60.
[27] S. Deville, E. Maire, A. Lasalle, A. Bogner, C. Gauthier, J. Leloup, C. Guizard, In situ x-ray radiography and tomography observations of the solidification of aqueous alumina particle suspensions—part I: initial instants, Journal of the American Ceramic Society 92 (11) (2009) 2489–2496.
[28] A. Lasalle, C. Guizard, J. Leloup, S. Deville, E. Maire, A. Bogner, C. Gauthier, J. Adrien, L. Courtois, Ice-templating of alumina suspensions: effect of supercooling and crystal growth during the initial freezing regime, Journal of the American Ceramic Society 95 (2) (2012) 799–804.
[29] R.W. Rice, Comparison of stress concentration vs. minimum solid area based mechanical property-porosity relations, Journal of Materials Science 28 (8) (1993) 2187–2190.
[30] Z. Huan, J. Chang, J. Zhou, Low-temperature fabrication of macroporous scaffolds through foaming and hydration of tricalcium silicate paste and their bioactivity, Journal of Materials Science 45 (4) 961–968.